Supplementary Information (SI) for Soft Matter.

Supplementary Information: Compound Giant Unilamellar Vesicle as Models for Electrohydrodynamics of Artifical Nucleate Cells

Rupesh Kumar[1], Rajarshi Chakrabarti[2], and Rochish M. Thaokar[3,*]

[1]Centre for Research in Nanotechnology & Science, Indian Institute of Technology Bombay, Mumbai 400076, Maharashtra, India
[2]Department of Chemistry, Indian Institute of Technology Bombay, Mumbai 400076, Maharashtra, India
[3]Department of Chemical Engineering, Indian Institute of Technology Bombay, Mumbai 400076, Maharashtra, India
[*]Correspondence: rochish@che.iitb.ac.in (Rochish M. Thaokar)

S1 MEMBRANE CHARGING TIME AND MAXWELL WAGNER RELAXATION TIME OF OUTER AND INNER VESICLE MEMBRANE

The charging and Maxwell Wagner times are given by (1)

$$t_{co} = R_o C_{mo}\left(\frac{1}{\sigma_a} + \frac{1}{2\sigma_o}\right) \tag{S.1}$$

$$t_{MWo} = \left(\frac{\epsilon_a + 2\epsilon_o}{\sigma_a + 2\sigma_o}\right) \tag{S.2}$$

$$t_{ci} = R_i C_{mi}\left(\frac{1}{\sigma_i} + \frac{1}{2\sigma_a}\right) \tag{S.3}$$

$$t_{MWi} = \left(\frac{\epsilon_i + 2\epsilon_a}{\sigma_i + 2\sigma_a}\right) \tag{S.4}$$

and are also detailed in the main article. Consistent parameters, including the capacitance of the inner and outer membranes, were used as specified in the model parameters section of the main article to compute the charging and Maxwell-Wagner time.

The determination of the charging and Maxwell-Wagner time for the outer and inner membranes involves calculations based on the radii of the undeformed cGUV (compound Giant Unilamellar Vesicle). These computed values are subsequently incorporated into the AR (Aspect Ratio) versus frequency plots presented in the main article. In the table S1 and S2, charging and Maxwell-Wagner time of outer and inner vesicles are reported using the radii of a representative cGUV for each case. Given the relatively minor variation in the radii of the other cGUVs, the charging and Maxwell-Wagner times of other cGUVs typically fall within a comparable range in each case.

Table S1: Charging time for outer and inner vesicle membrane of cGUV

σ_o (μS/cm)	σ_a (μS/cm)	σ_i (μS/cm)	R_i (μm)	R_o (μm)	t_{ci}^{-1} (kHz)	t_{co}^{-1} (kHz)
4	4	4	8.9	17.1	8.6	4.46
4	12	4	8.2	16	11.9	8.57
24	4	4	6.2	12.8	12.3	8.24
72	12	4	4.9	11.7	20.0	27.05
24	4	24	7.5	16.7	22.9	6.32
13	18	65	5.4	9.4	122.6	32.33

S2 UNSTEADY STATE CONDITION

Apart from the case of $\sigma_i < \sigma_a > \sigma_o$ discussed in detail in the main article, unsteady state deformation for the rest of the five cases is reported in the figure S1. The aspect ratio (AR) evolution with time for experimental data is compared with the

Table S2: Maxwell Wagner time for outer and inner vesicle membrane of cGUV

σ_o (μS/cm)	σ_a (μS/cm)	σ_i (μS/cm)	R_i (μm)	R_e (μm)	t_{MWi}^{-1} (kHz)	t_{MWo}^{-1} (kHz)
4	4	4	8.9	17.1	564.7	564.7
4	12	4	8.2	16	1317.7	941.2
24	4	4	5.8	13.6	564.7	2447.1
72	12	4	4.9	11.7	1317.7	7341.3
24	4	24	7.5	16.7	1505.9	2447.1
13	18	65	5.4	9.4	4753.0	2070.6

theoretical predictions. The time required to achieve the steady state AR value is in reasonable qualitative agreement with the theoretical model. However, quantitatively, the experimental values of AR are seen to deviate from the model predictions for a variety of reasons discussed in the main article. In Fig. S1 the AR values reported are for electrodeformation studies at f=100 kHz for all the cases except experiments on cGUV without salt addition, that is ($\sigma_o = \sigma_a = \sigma_i$= 4 μS/cm) which was conducted at f= 500 Hz. The other parameters in all the studies are kept idential, with $E = 0.05KV/cm$, $C_{mo} = C_{mi} = 0.35$ $\mu F/cm^2$, $K_{bi} = K_{bo} = 50k_BT$ and membrane tension $\gamma_{ini} = 10^{-9}$ mN/m (2–5).

S3 TIME AVERAGED STATIONARY DEFORMATION

S3.1 AR vs frequency plots

The work presented in this article mostly focuses on understanding the variation of the time-averaged stationary deformation exhibited by the cGUVs under AC fields. While two datasets for each experimental condition were discussed in good detail in the main article, for each of these experimental conditions, at least 4-5 distinct cGUVs were investigated in Fig. S2 ($\sigma_o = 24, \sigma_a = 4, \sigma_i$= 24 μS/cm), Fig. S3 ($\sigma_o = 13, \sigma_a = 18, \sigma_i$= 65 μS/cm), Fig. S4 ($\sigma_o = 4, \sigma_a = 12, \sigma_i$= 4 μS/cm), Fig. S5 ($\sigma_o = 72, \sigma_a = 12, \sigma_i$= 4 μS/cm), all these figures illustrate the change in the AR vs frequency for both outer and inner vesicles. Each figure shows upper and lower plots depicting AR vs frequency for outer and inner vesicles, respectively.

While the data for the above cases, wherein the conductivity of any two adjacent media, inner and annular or outer and annular are different, give fairly consistent results, a sensitive dependence to preparation conditions is observed when either $\sigma_i = \sigma_a$ or $\sigma_o = \sigma_a$. For example, in Figure S6 in a cGUV with $\sigma_o = 24\mu S/cm$, $\sigma_a = 4\mu S/cm$, $\sigma_i = 4\mu S/cm$), the outer vesicle can exhibit prolate-oblate-sphere transition, and inner vesicles deform into a sphere-prolate-sphere transition (Fig. S6a), in agreement with theoretical predictions, in another experiment, while the outer vesicle continues to show prolate-oblate-sphere transition, the inner vesicle may now show a sphere-prolate-oblate-sphere transition (Fig. S6b). This can be attributed to a marginally higher electrical conductivity in the annular region compared to the inner region of the cGUV.

Likewise, in Figure S7, for $\sigma_o = 4\mu S/cm$, $\sigma_a = 4\mu S/cm$, $\sigma_i = 4\mu S/cm$, the inner vesicle can show prolate (Fig. S7a) and occasionally oblate deformation (Fig. S7b) at intermediate frequency, depending on a particular experimental run. In Fig. S7a, inner vesicles are highly deformable under osmotic shock, as in normal conditions, very small deforms are observed. A small deformation (AR<1.05) was observed in the inner vesicles if its radius is less than 7 μm, larger size inner vesicle with radius 12.8 μm shown in Fig. S7c exhibit significant deformation. When conductivities are not maintained, inner vesicles transit to spherical-prolate-oblate-spherical shape that matched with a theoretical model shown in Fig. S7c through adjusting a conductivity condition to $\sigma_o = 4.2\mu S/cm$, $\sigma_a = 4.2\mu S/cm$, $\sigma_i = 4\mu S/cm$, adjusting a conductivities with a such a small values outer and inner vesicle electrodeformation pattern shows reasonable qualitative agreement in Fig. S7c.

S3.2 Analysing integrity of cGUV during AC deformation

Possible structural changes, including unfurling of loosely bound regions of the bilayer membrane in a cGUV or irreversible changes in a cGUV undergoing electrodeformation are reported in two different experiments. In the first experiment, Figure S8, a cGUV undergoes electrodeformation in forward frequency sweep of 100 Hz to 10 MHz, followed by a reverse frequency sweep from 10 MHz back to 100 Hz, for assessing vesicle integrity. Figure S8 illustrates a plot plotting the AR vs frequency during electrodeformation, generated through forward and reverse frequency sweeps. The observation of comparable AR values at each frequency point during both the forward and reverse electrodeformation cycles suggests consistent deformability of

cGUV and very little unfolding/unfurling during short runs of experiments. Several experiments on many different cGUVs under varied conductivity ratios showed such behavior.

However, notable deviations from theoretical results, were obtained in the vesicle electrodeformation behavior in a few cases. Figure S9 shows that while the inner vesicle exhibits reasonable values of deformation, the outer vesicle, while admiting prolate deformation, consistent with theoretical predictions, however, displays abnormally high AR values. Such instances indicate a possible tendency towards "softening and unfurling" of the bilayer during electrodeformation, rendering these vesicles unsuitable for further analysis.

S4 TMP, NORMAL AND TANGENTIAL ELECTRIC STRESSES

The experimental results in the main paper are exhaustively explained using the variation of TMP, normal and tangential stresses as obtained from theoretical calculations (6) for the case of $\sigma_o = \sigma_i = 4\mu S/cm, \sigma_a = 12\mu S/cm$. A similar approach can be taken to understand all the the experimental results presented in the main manuscript, using the variation of TMP, normal and tangential electric stresses, as predicted by the theory, for various cases of conductivities in the three regions, considered in this work. These are presented in figures S10,S11,S12,S13 and S14.

S5 ANALYSIS OF CGUV MORPHOLOGY USING MICROSCOPY

A vesicular solution consisting of sGUVs, when subjected to an osmotic shock, transforms into a diverse population of vesicles within half an hour Fig. S15a. This vesicular solution shows multiple morphologies such as vesicle-in-vesicle cGUVs, multiple vesicles-in-vesicle cGUVs, non-spherical cGUVs and tubular structures. The normal DIC image of the vesicular solution at 3 hours Fig S15b also does not seem to confirm well separateness of the inner and outer vesicles of the cGUVs.

The normal DIC images of the vesicular solution, taken at the end of half an hour (S15a) and 3 hours (S15b) do not seem to clearly show any difference between the well separateness of the inner and outer vesicle of the cGUV at the end of half an hour, or at the end of 3 hours. Therefore confocal microscopy is conducted Fig. S17 on single cGUVs. Similarly DIC imaging is also conducted on single cGUVs with the microscope focused at a lower plane.

Figure S16 shows the confocal microscopy and DIC images of an intermediate state cGUV at the end of half an hour. The figure clearly shows that the inner vesicle is attached to the outer vesicle through a visible neck in this intermediate state, and the connecting neck is visible in both fluorescent and DIC images shown in Fig. S16 with the microscope focused at a lower plane. If the microscope is focused at the equatorial plane though, it may be wrongly concluded that the inner and outer vesicles are well separated.

Figure S17 shows DIC and confocal microscopy at the end of 3 hours. In most of the cGUVs at this point, well separated inner and outer vesicles are seen in the cGUV, both at lower and at equatorial planes, and in both confocal and DIC microscopy. This suggests that the intermediate state of stomatocytes and cGUVs with neck connected inner vesicles, undergo transition to a state where the inner vesicle is completely separated from the outer vesicle over a timescale of around 3 hours, and the interconnecting neck is found to disappear.

Around fifty such cGUVs were imaged after 3 hours, and all showed a well-separated inner vesicle from the outer vesicle. Once the neck is pinched and anhiliated, the inner vesicle seems to separate from the outer vesicles and moves upwards in the cGUV due to buoyancy (inner vesicle has a mixture of glucose and sucrose while the annular space has sucrose) and is shown in Fig. S17 and in Fig. S18 using 3D images at different orientations. The figures clearly show that in well-formed cGUVs, the cGUVs have no connection between the inner and outer vesicles through any visible lipid tube. Other morphologies of cGUVs, such as multiple inner vesicles are shown in Fig. S19 and small internal liposomes and tubules with larger inner vesicles in the cGUVs, are clearly seen in these images. In some rare instances, subsequent to the formation of cGUVs, a notable osmolarity mismatch persisted in the inner and annular region of the cGUVs. This disparity can lead to further restructuring of the inner vesicles into stomatocytes and the eventual generation of concentric triple vesicles (vescile-in-vesicle-in-vesicle), as illustrated in Figure S20.

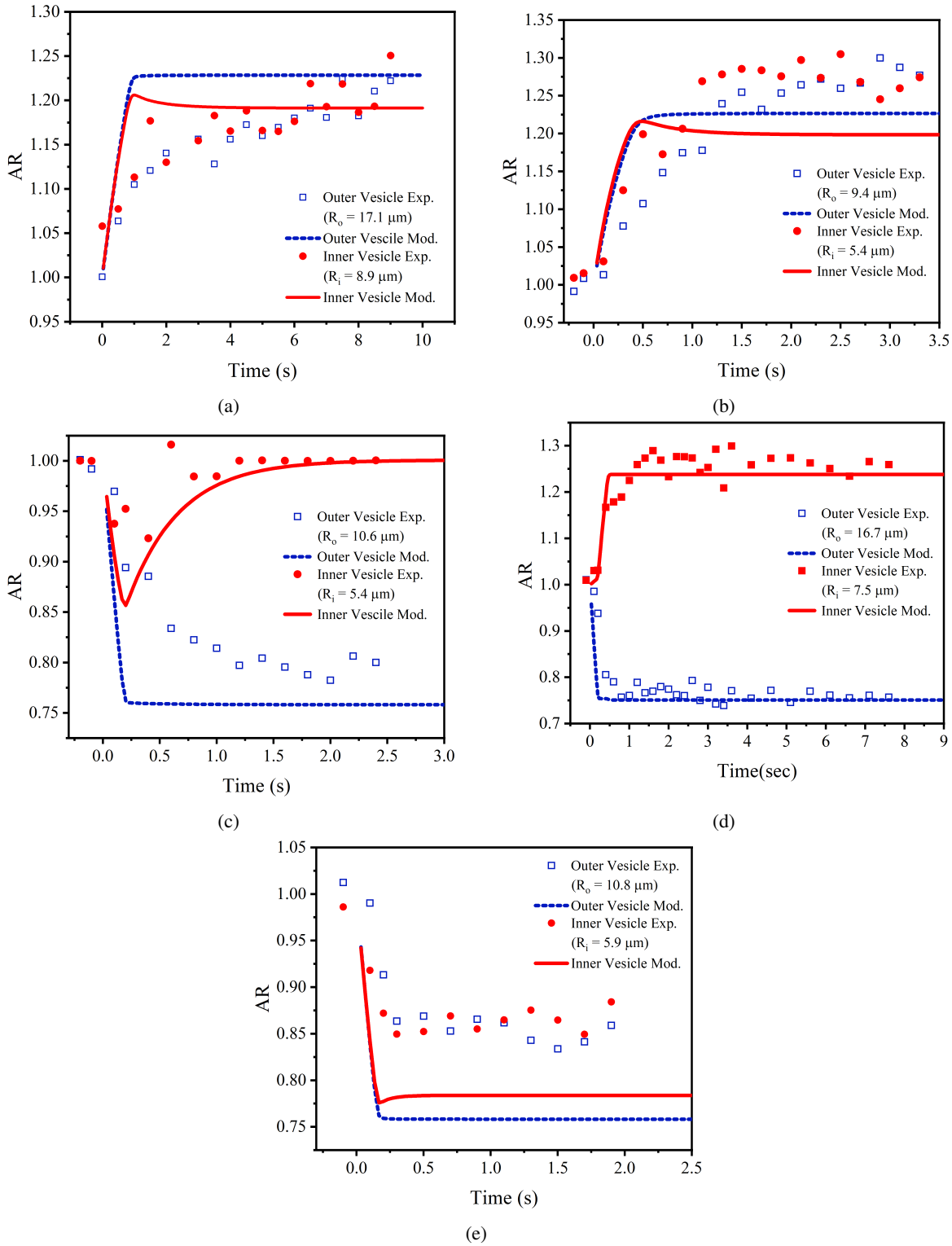

Figure S1: Unsteady state AC deformation at various electrical conductivity conditions. Increase in deformation of inner and outer vesicles of cGUVs with time, and changes in an aspect ratio of inner and outer vesicles of cGUVs with time. (a) $\sigma_o = 4\mu S/cm$, $\sigma_a = 4\mu S/cm$, and $\sigma_i = 4\mu S/cm$, (b) $\sigma_o = 13\mu S/cm$, $\sigma_a = 18\mu S/cm$, and $\sigma_i = 65\mu S/cm$, (c) $\sigma_o = 24\mu S/cm$, $\sigma_a = 4\mu S/cm$, and $\sigma_i = 4\mu S/cm$, (d) $\sigma_o = 24\mu S/cm$, $\sigma_a = 4\mu S/cm$, $\sigma_i = 24\mu S/cm$ and (e) $\sigma_o = 72\mu S/cm$, $\sigma_a = 12\mu S/cm$, $\sigma_i = 4\mu S/cm$. The continuous line (theoretical model values) and symbols (experimental values).

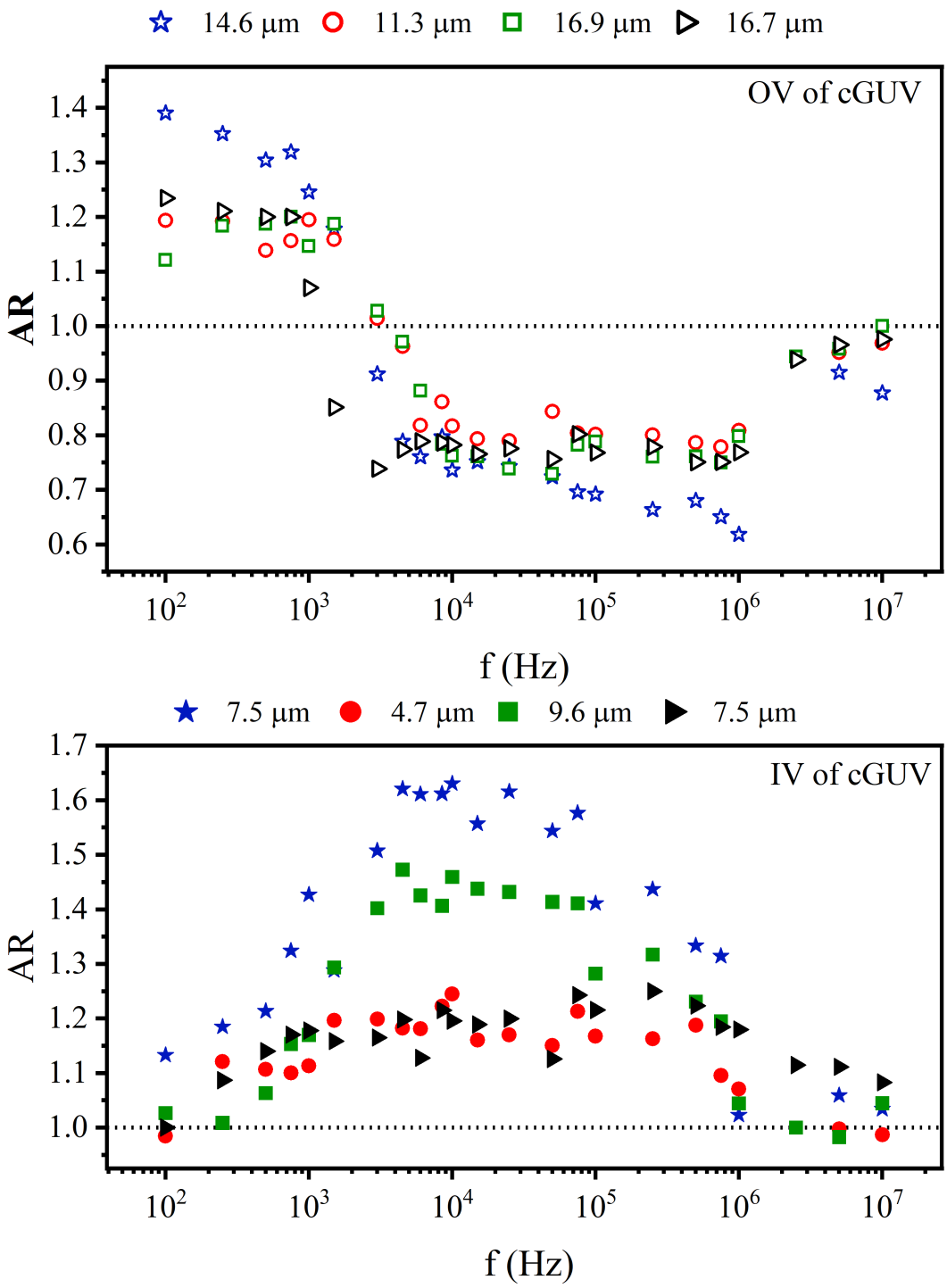

Figure S2: AR vs f for $\sigma_o = 24\mu S/cm$, $\sigma_a = 4\mu S/cm$, $\sigma_i = 24\mu S/cm$, $E_o = 0.05kV/cm$. The hollow symbols in the upper plot are for outer vesicles, and the filled symbols in the lower plot are for inner vesicles in each plot.

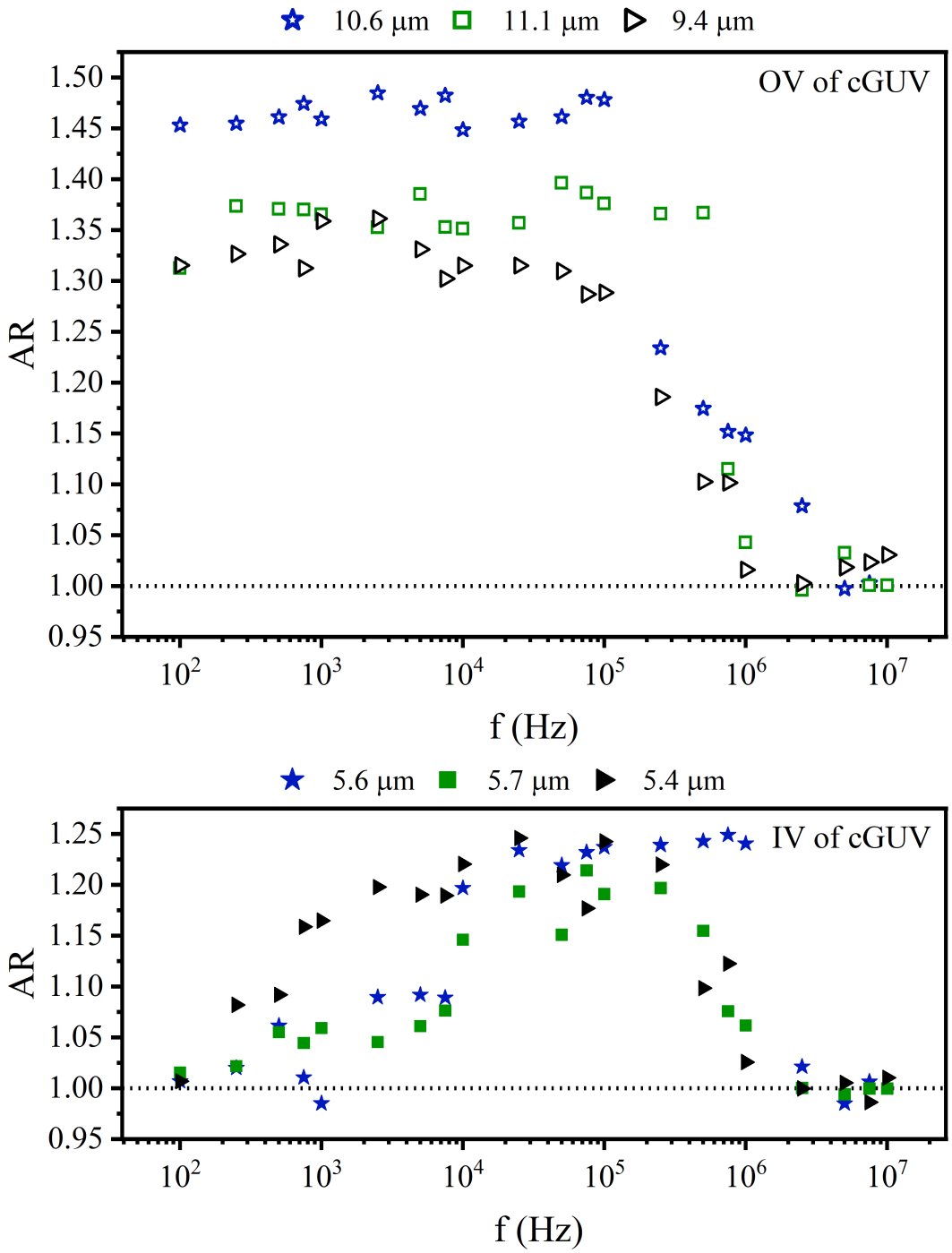

Figure S3: AR vs f for $\sigma_o = 13\mu S/cm$, $\sigma_a = 18\mu S/cm$, $\sigma_i = 65\mu S/cm$, $E_o = 0.05KV/cm$. The hollow symbols in the upper plot are for outer vesicles, and the filled symbols in the lower plot are for inner vesicles in each plot.

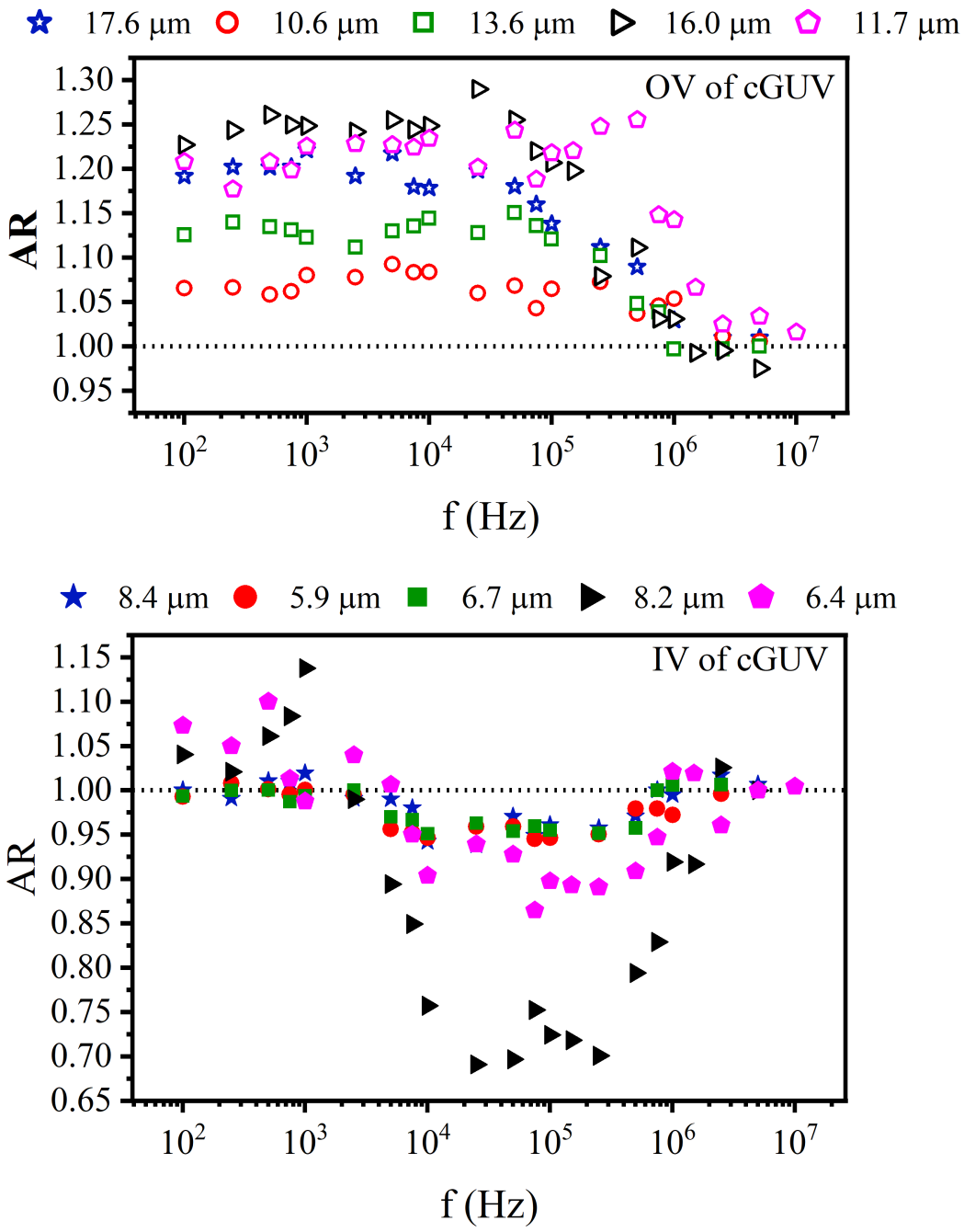

Figure S4: AR vs f for $\sigma_o = 4\mu S/cm$, $\sigma_a = 12\mu S/cm$, $\sigma_i = 4\mu S/cm$, $E_o = 0.05KV/cm$. The hollow symbols in the upper plot are for outer vesicles, and the filled symbols in the lower plot are for inner vesicles in each plot.

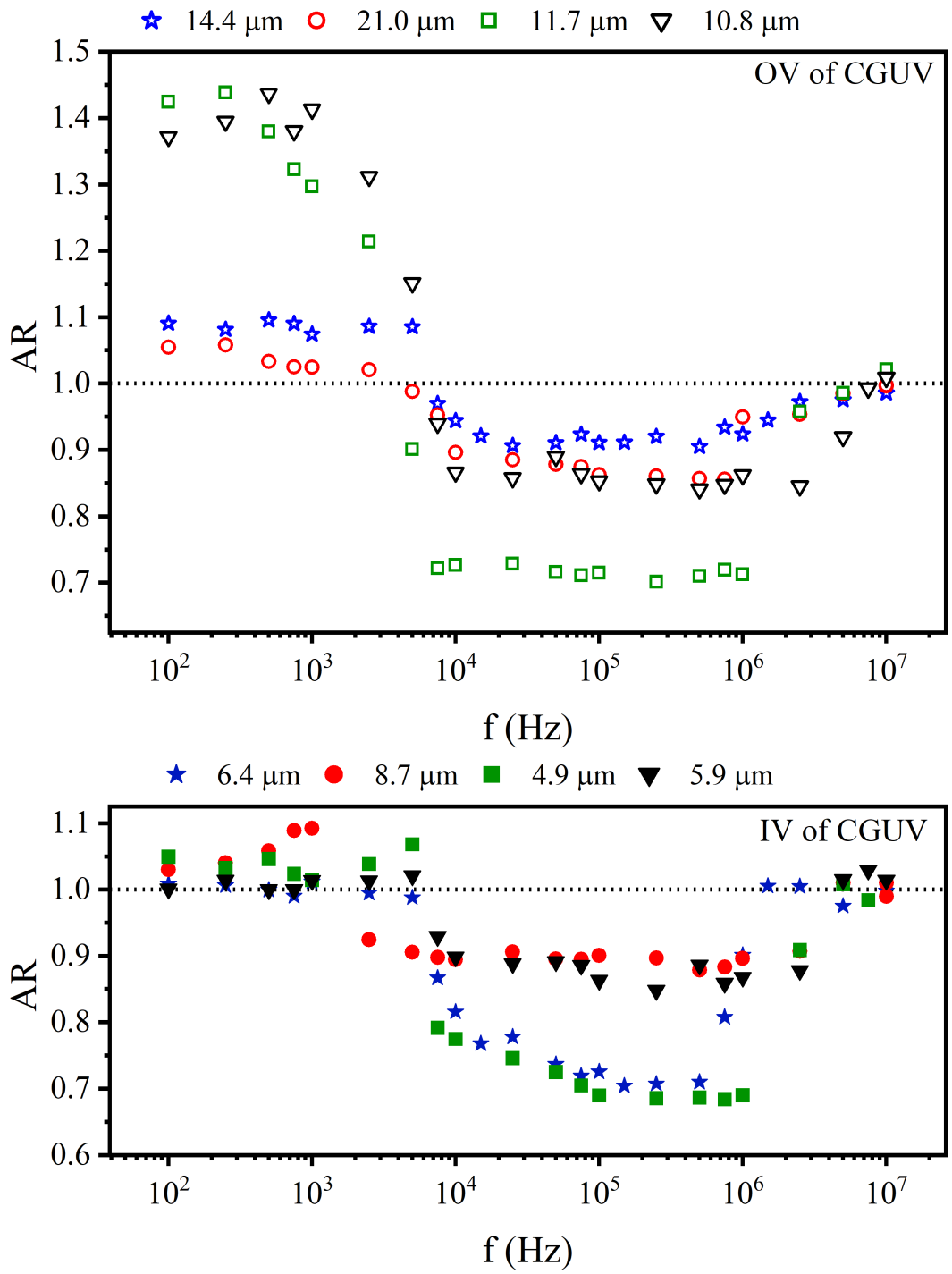

Figure S5: AR vs f for $\sigma_o = 72\mu S/cm$, $\sigma_a = 12\mu S/cm$, $\sigma_i = 4\mu S/cm$, $E_o = 0.05KV/cm$. The hollow symbols in the upper plot are for outer vesicles, and the filled symbols in the lower plot are for inner vesicles in each plot.

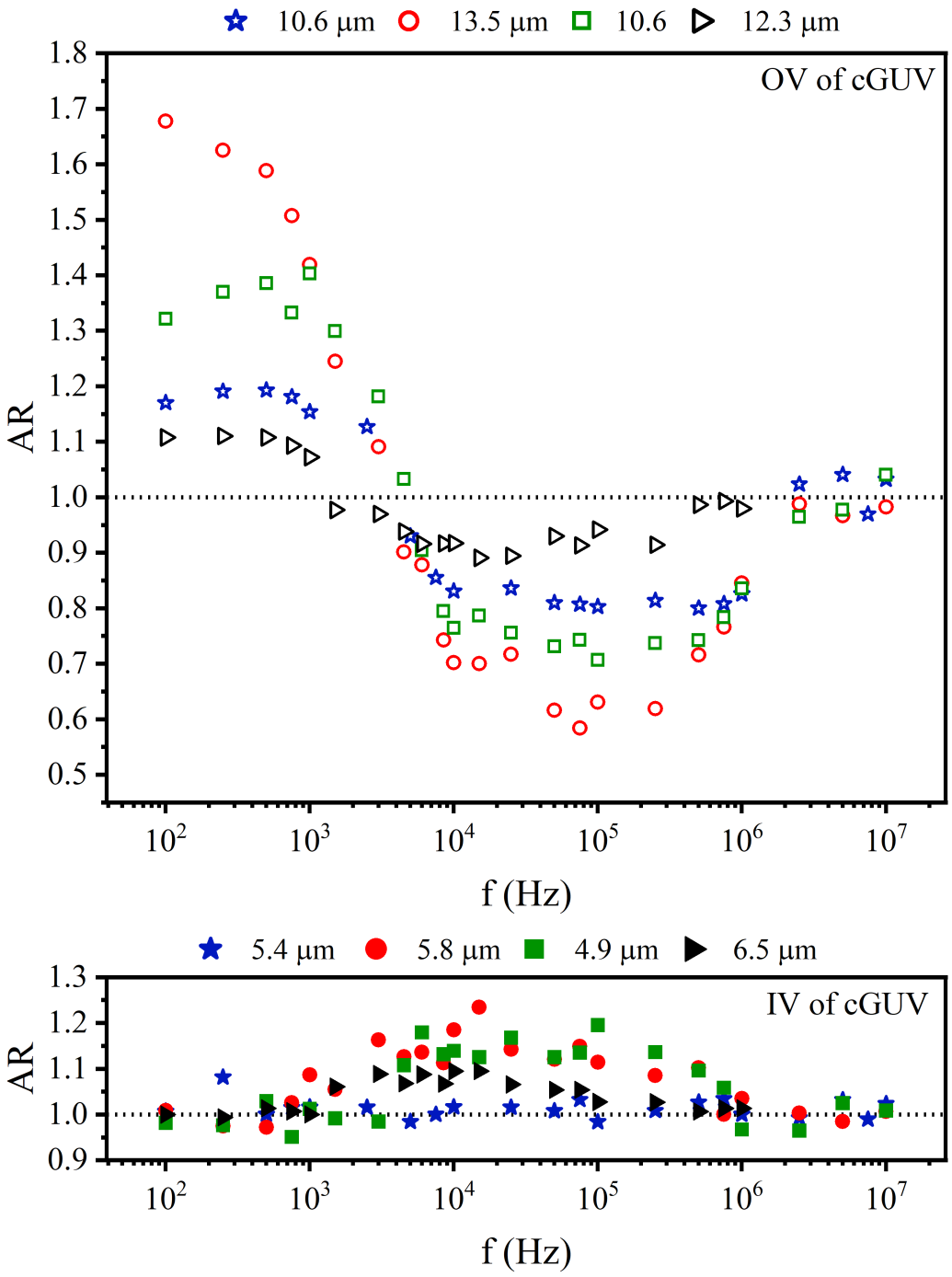
10.6 µm
13.5 µm
10.6
12.3 µm
OV of cGUV
AR
f (Hz)
5.4 µm
5.8 µm
4.9 µm
6.5 µm
IV of cGUV
AR
f (Hz)

(a)

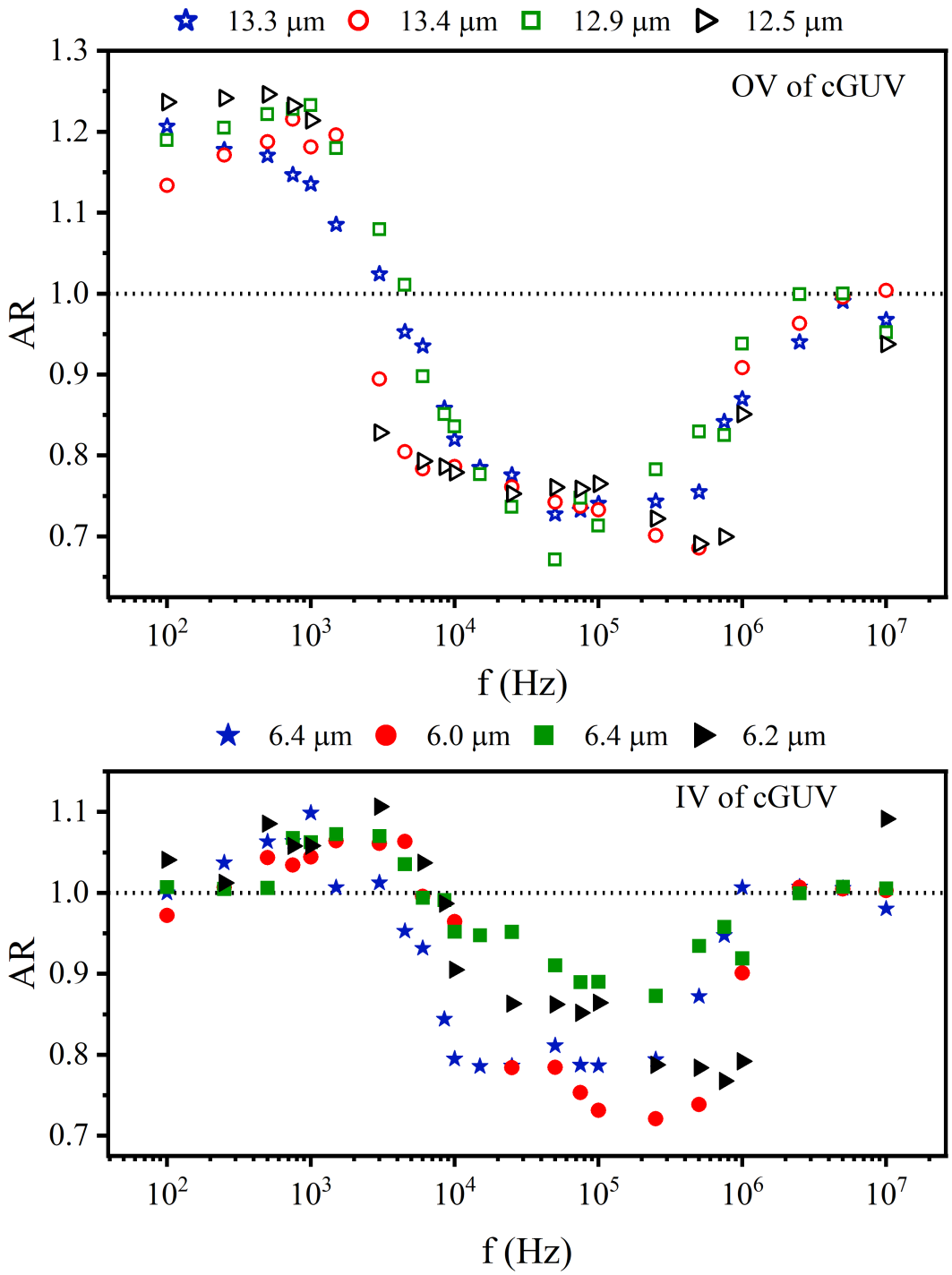

(b)

Figure S6: AR vs f for $\sigma_i = \sigma_a = 4\mu S/cm$, $\sigma_o = 24\mu S/cm$, $E_o = 0.05KV/cm$ (a) Conductivities get accurately maintained (b) When the conductivity condition cannot be not maintained accurately, the annular region has slightly higher conductivity than the inner region.

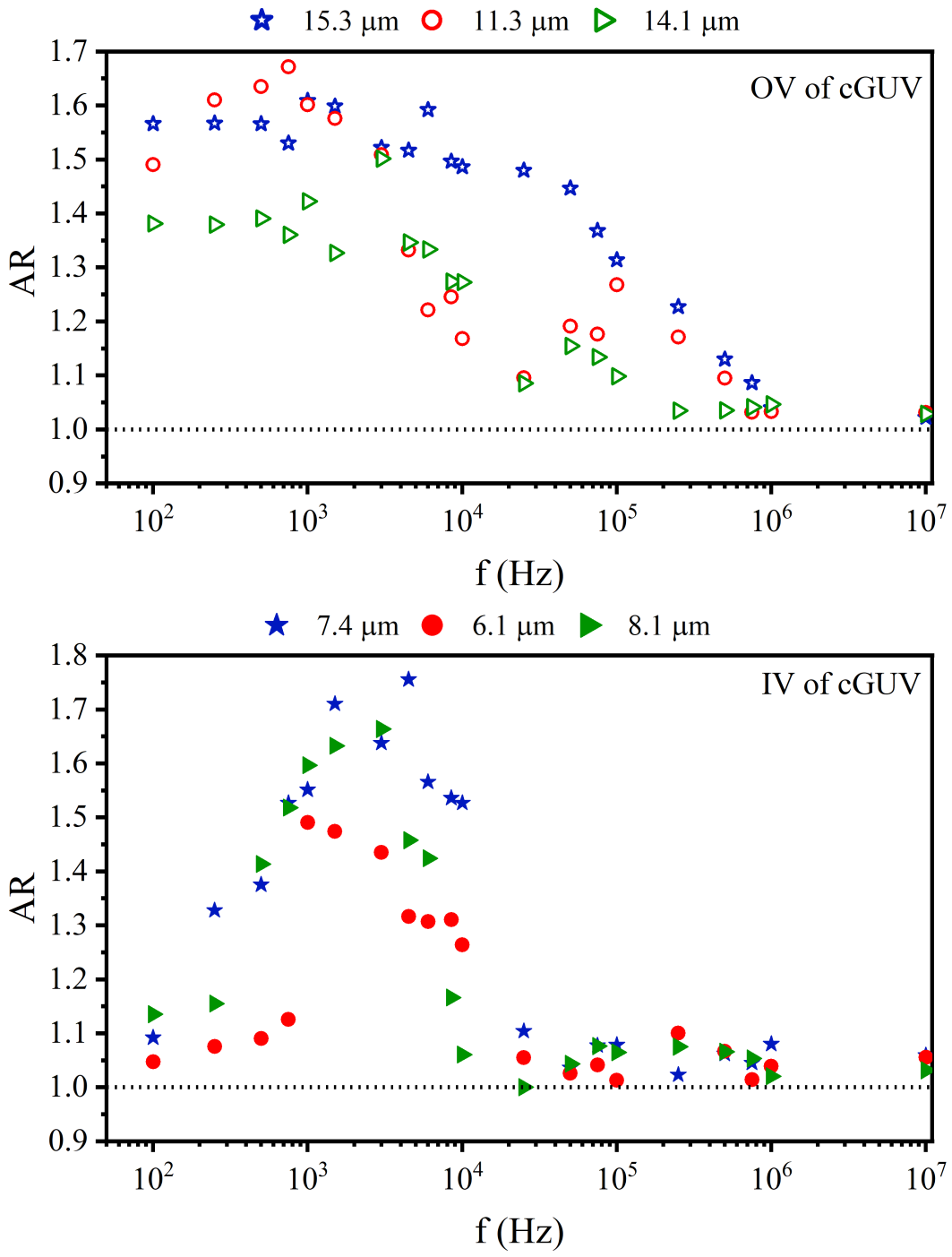
15.3 µm
11.3 µm
14.1 µm
OV of cGUV
AR
f (Hz)
7.4 µm
6.1 µm
8.1 µm
IV of cGUV
AR
f (Hz)

(a)

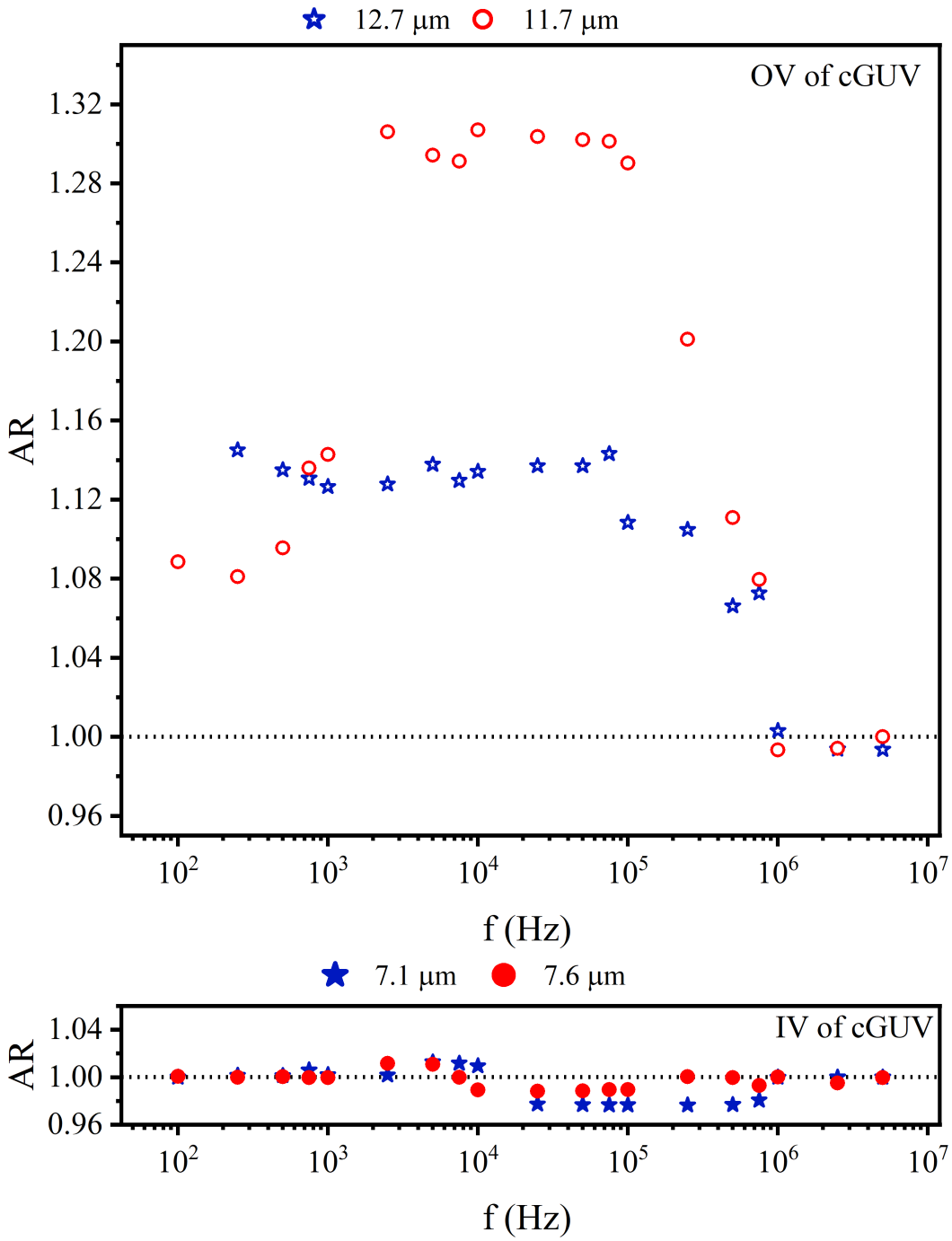
12.7 µm
11.7 µm
OV of cGUV
AR
1.32
1.28
1.24
1.20
1.16
1.12
1.08
1.04
1.00
0.96
10^2
10^3
10^4
10^5
10^6
10^7
f (Hz)
7.1 µm
7.6 µm
IV of cGUV
AR
1.04
1.00
0.96
10^2
10^3
10^4
10^5
10^6
10^7
f (Hz)

(b)

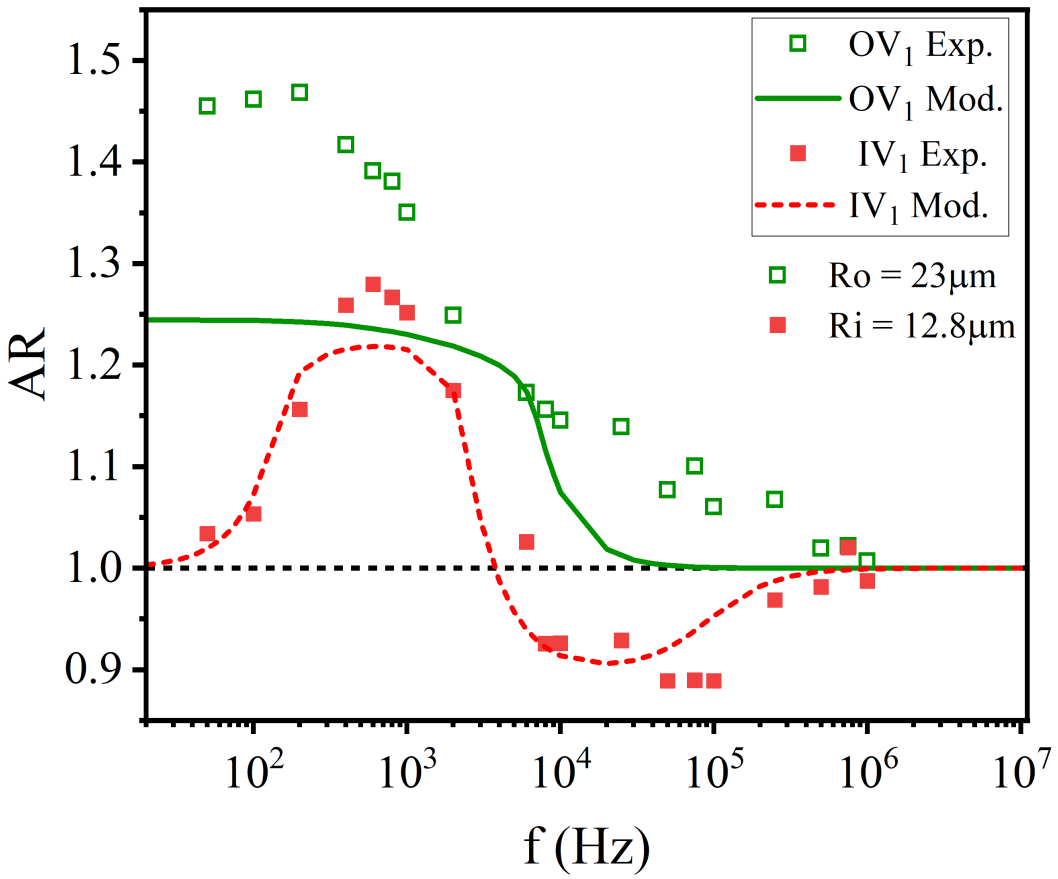

(c)

Figure S7: AR vs f for $\sigma_o = 4\mu S/cm$, $\sigma_a = 4\mu S/cm$, $\sigma_i = 4\mu S/cm$, $E_o = 0.05KV/cm$ (a) Conductivity condition gets accurately maintained, the membrane becomes highly deformable through osmotic stress (b) When the conductivity condition cannot be not maintained, the annular region has slightly higher conductivity than the inner region (c) Theoretical model and experimental result are compared when the conductivity is not maintained (values of conductivities in theoretical model are $\sigma_o = 4.2\mu S/cm$, $\sigma_a = 4.2\mu S/cm$, $\sigma_i = 4\mu S/cm$) .

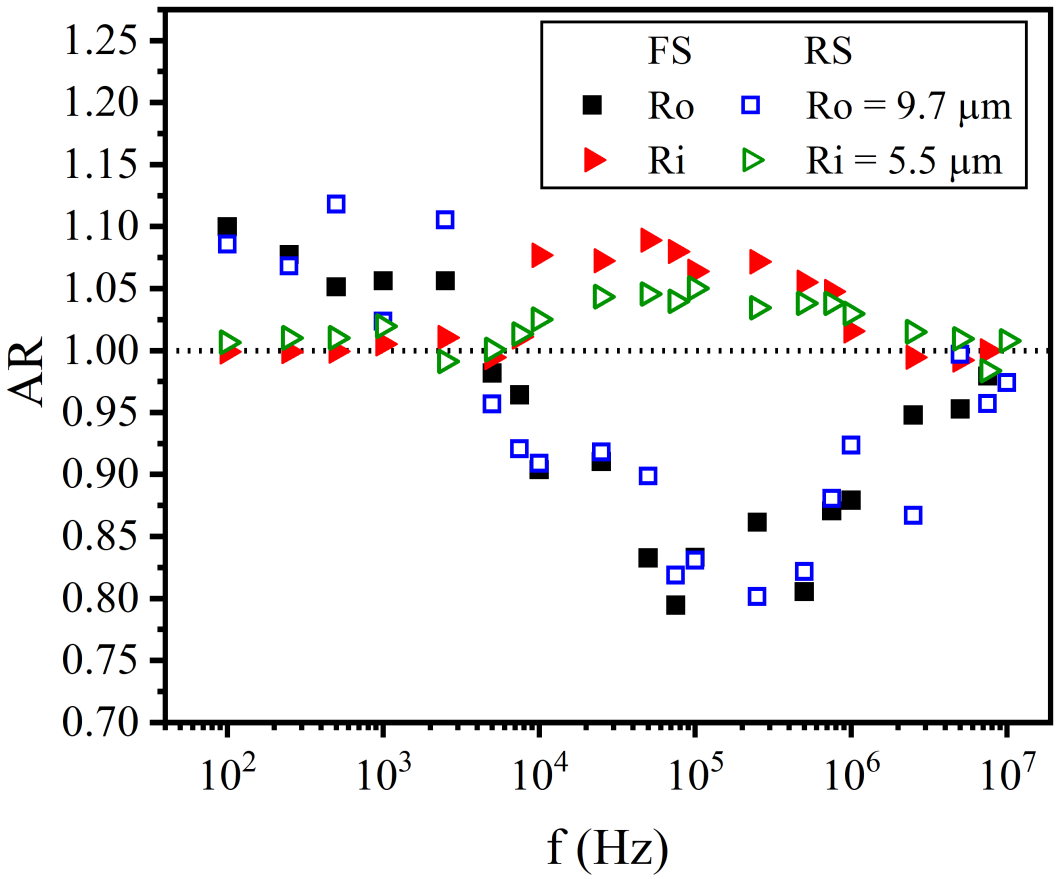

Figure S8: Reproducibility of deformation of the same cGUV during increasing and decreasing frequency sweep for all other conditions kept identical in an experiment (a) Forward frequency sweep, 100Hz to 10MHz (b) Reverse sweep, 10MHz to 100Hz. Here, $E = 0.05 KV/cm$, σ_o =24 μS/cm, σ_a =4 μS/cm, σ_i = 24 μS/cm. Scattered plot (expts), solid line (model values), FS = Forward Sweep and RS = Reverse Sweep.

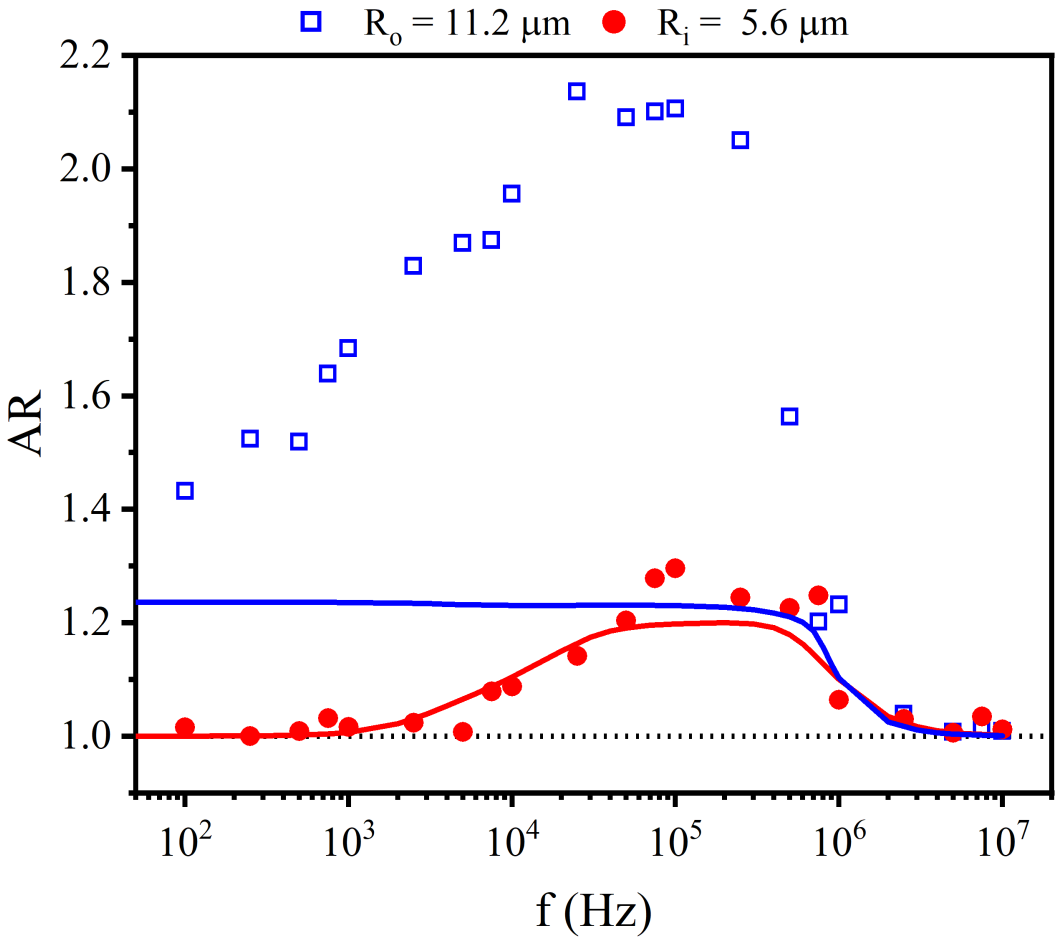

Figure S9: AR vs f is plotted for $\sigma_o = 13\mu S/cm$, $\sigma_a = 18\mu S/cm$, $\sigma_i = 65\mu S/cm$, $E_o = 0.05KV/cm$. The outer vesicle shows abnormally high AR values at intermediate frequencies, showing inconsistent deformability. Fitted initial tension (γ_{ini}) for outer and inner vesicle = $10^{-9}mN/m$, scattered plot (Expts) and solid line (model values).

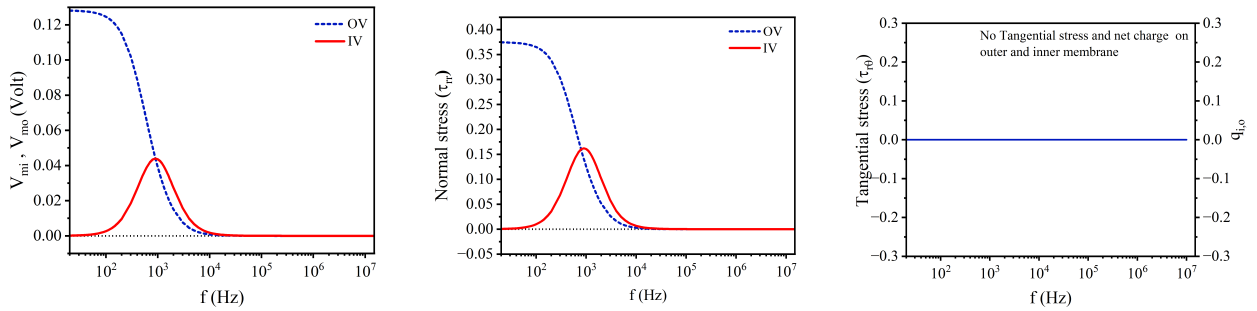

Figure S10: Variation with frequency of (a) Transmembrane potential for outer (V_{mo}) and inner (V_{mi}) vesicles (b) Normal stress τ_{rr} on outer and inner vesicles and (c) Tangential stress $\tau_{r\theta}$ on outer and inner vesicles. ($\sigma_o = 4\mu S/cm$, $\sigma_a = 4\mu S/cm$, $\sigma_i = 4\mu S/cm$, $R_i = 8.9\mu$m, $R_o = 17.1\mu$m, $E_o = 0.05kV/cm$). The electric stress is normalised by $\epsilon_o E_o^2 \sim 0.018N/m^2$. The charge density is scaled by $\epsilon_o E_o \sim 10^{-6}pC/\mu m^2$. OV-Outer Vesicle, IV-Inner Vesicle.

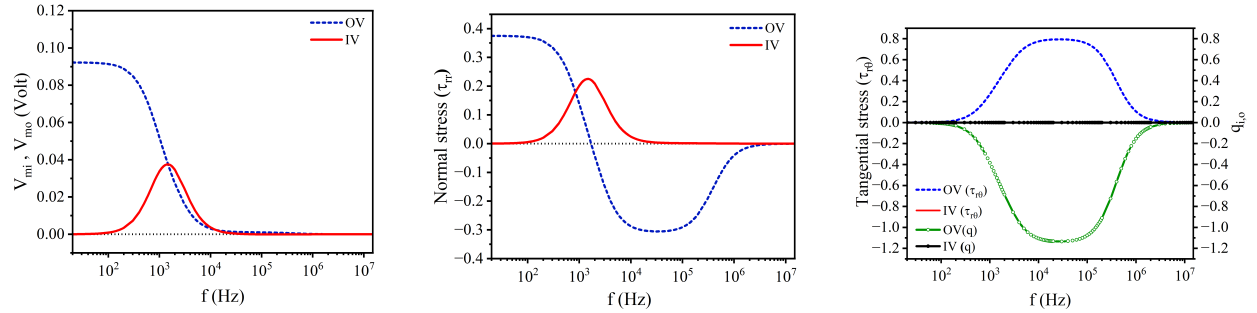

Figure S11: Variation with frequency of (a) Transmembrane potential for outer (V_{mo}) and inner (V_{mi}) vesicles (b) Normal stress (τ_{rr}) on outer and inner vesicles (c) Tangential ($\tau_{r\theta}$) stress on outer and inner vesicles. (σ_o = 24 μS/cm, σ_a = 4 μS/cm and σ_i = 4 μS/cm, R_i = 5.8 μm, R_o = 13.6 μm, $E_o = 0.05KV/cm$). The IV ($\tau_{r\theta}$) and IV (q) are overlapped. The electric stress is normalised by $\epsilon_o E_o^2 \sim 0.018N/m^2$. The charge density is scaled by $\epsilon_o E_o \sim 10^{-6}pC/\mu m^2$. OV-Outer Vesicle, IV-Inner Vesicle.

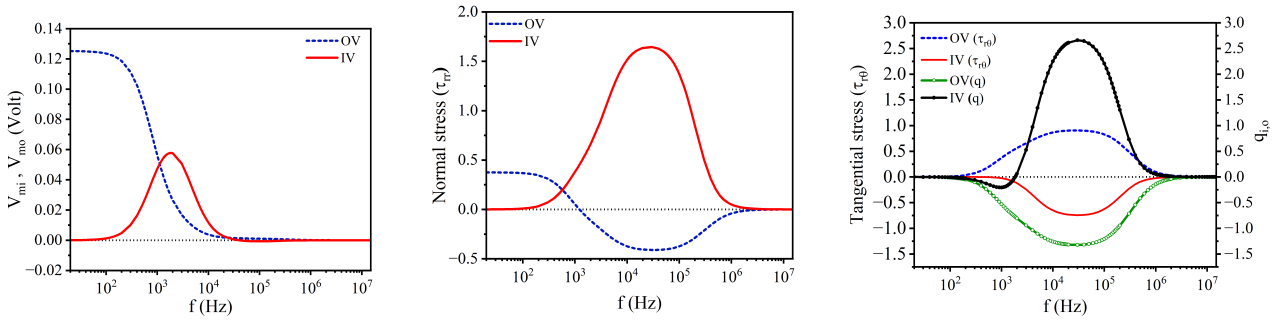

Figure S12: Variation with frequency of (a) Transmembrane potential for outer (V_{mo}) and inner (V_{mi}) vesicles (b) Normal stress (τ_{rr}) on outer and inner vesicles (c) Tangential stress ($\tau_{r\theta}$) on outer and inner vesicles. (σ_o = 24 μS/cm, σ_a = 4 μS/cm and σ_i = 24 μS/cm, R_i = 7.5 μm, R_o = 16.7 μm, $E_o = 0.05KV/cm$). The electric stress is normalised by $\epsilon_o E_o^2 \sim 0.018N/m^2$. The charge density is scaled by $\epsilon_o E_o \sim 10^{-6}pC/\mu m^2$. OV-Outer Vesicle, IV-Inner Vesicle.

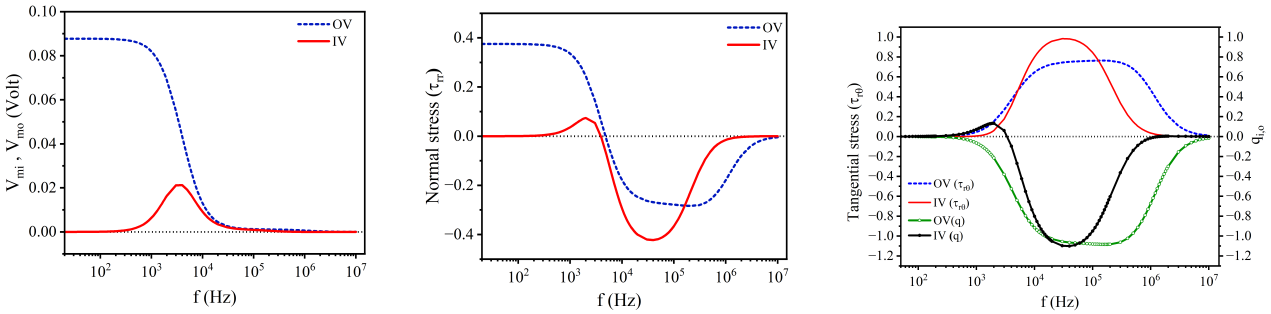

(a) (b) (c)

Figure S13: Variation with frequency of (a) Transmembrane potential for outer (V_{mo}) and inner (V_{mi}) vesicles (b) Normal stress (τ_{rr}) on outer and inner vesicles (c) Tangential stress ($\tau_{r\theta}$) on outer and inner vesicles (σ_o = 72 μS/cm, σ_a = 12 μS/cm and σ_i = 4 μS/cm, R_i = 4.9 μm, R_o = 11.7 μm, E_o = $0.05KV/cm$). The electric stress is normalised by $\epsilon_o E_o^2 \sim 0.018N/m^2$. The charge density is scaled by $\epsilon_o E_o \sim 10^{-6} pC/\mu m^2$. OV-Outer Vesicle, IV-Inner Vesicle.

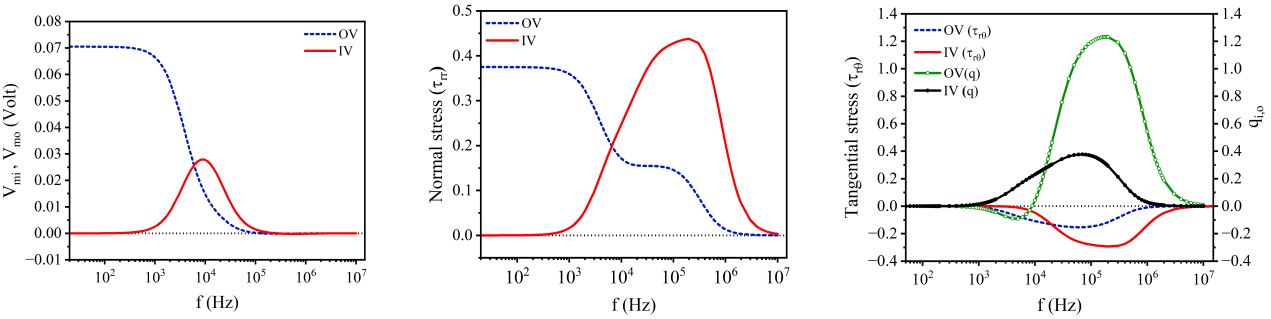

(a) (b) (c)

Figure S14: Variation with frequency of (a) Transmembrane potential for outer (V_{mo}) and inner (V_{mi}) vesicles (b) Normal stress (τ_{rr} on outer and inner vesicles (c) Tangential stress ($\tau_{r\theta}$) on outer and inner vesicles (σ_o = 13 μS/cm, σ_a = 18 μS/cm and σ_i = 65 μS/cm, R_i = 5.4μm, R_o = 9.4μm, E_o = $0.05KV/cm$). The electric stress is normalised by $\epsilon_o E_o^2 \sim 0.018N/m^2$. The charge density is scaled by $\epsilon_o E_o \sim 10^{-6} pC/\mu m^2$. OV-Outer Vesicle, IV-Inner Vesicle.

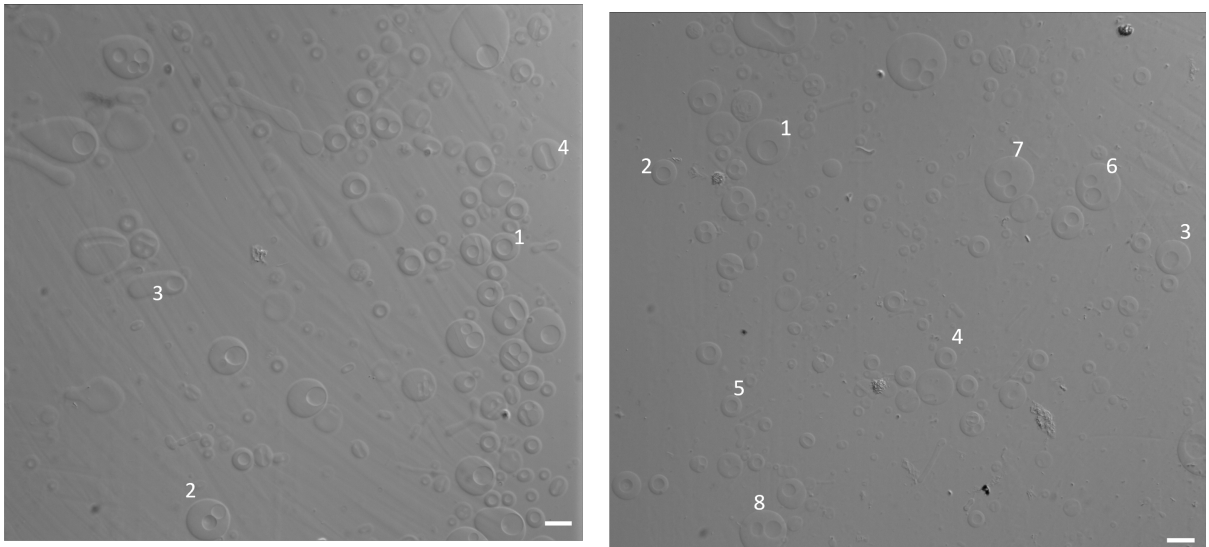

(1) single inner vesicle (2) multiple inner vesicles (3) non-spherical outer vesicle (4) non-spherical inner vesicle

(a)

(1,2,3,4,5) single inner vesicle (6,7,8) multiple inner vesicles

(b)

Figure S15: sGUV Vesicular subjected to an osmotic shock (a) A large window of sample imaged after around half an hour of osmotic in which the major population of vesicular structures are vesicle-in-vesicle cGUVs, multiple vesicle-in-vesicle cGUVs, non-sphereical cGUVs (b) cGUV imaged after 3 hours to ascertain integrity of the cGUV formed. (a) and (b) are images of the same sample at different locations. Scale bar = 30 μm.

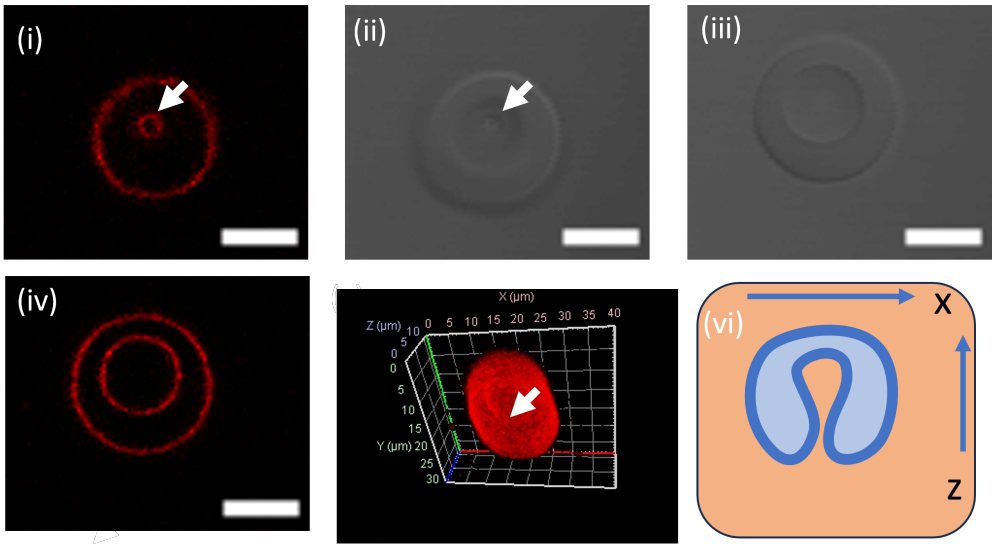

Figure S16: Morphology of cGUV in intermediate state. Inner vesicle connected to the outer: (i) and (ii) shows fluorescent and DIC image at a lower z (height) and plane where neck is visible (white arrow) in both fluorescent and DIC image. (iii) and (iv) show a fluorescent and DIC image with cGUV in the equatorial plane. (v) 3D constructed image of an intermediate stage where the neck is shown with a white arrow. Scale bar = 10 μm

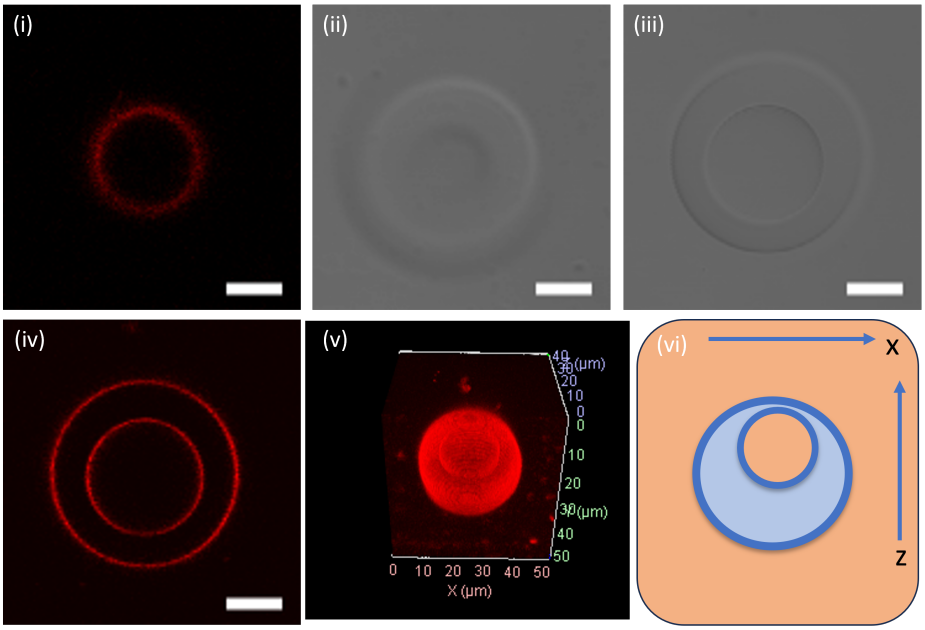

Figure S17: Morphology of a cGUV with completely separated inner and outer vesicle: (i) and (ii) fluorescent and DIC image at lower z plane of the cGUV where only outer vesicles are visible. (iii) and (iv) fluorescent and DIC image at an equatorial plane. (v) 3D constructed image of cGUV. Scale bar = 10 μm.

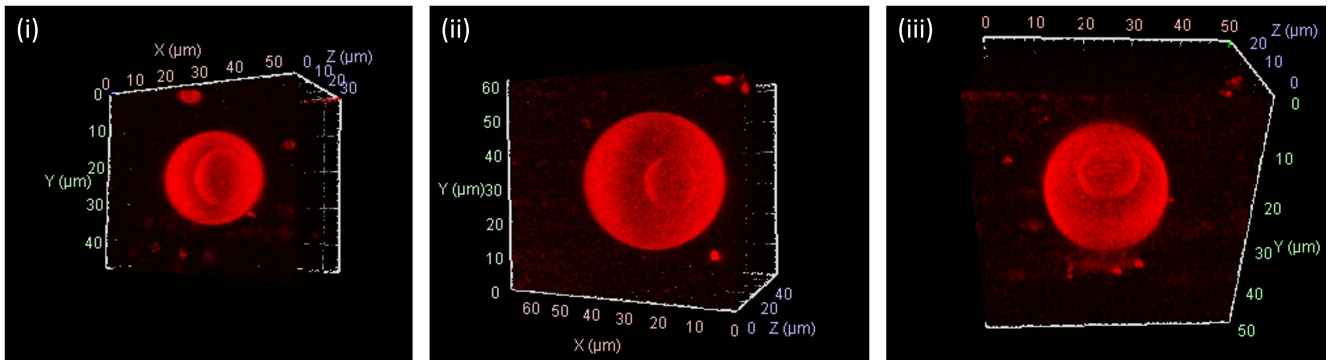

Figure S18: 3D image of a cGUV with a separated inner and outer vesicle are shown in (i), (ii), and (iii) at different orientations to show the position of the inner vesicle with respect to the outer vesicle. In all these cases, completely separated inner vesicles are positioned towards the top inside the cGUV, along the z-axis and appear to move in the xy-plane.

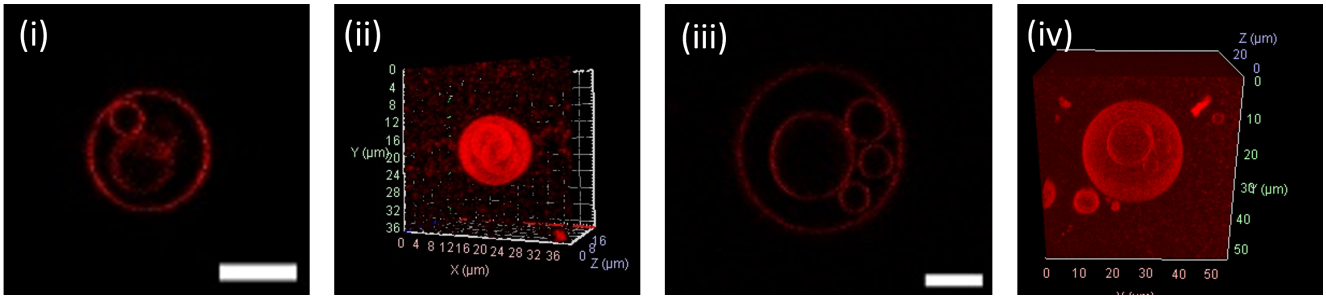

Figure S19: cGUV with multiple inner vesicles: (i) and (iii) fluorescent images at the equatorial plane and their respective 3D constructed images in (ii) and (iv) show a cGUV with multiple inner vesicles. All these vesicles appear to be completely separated from the outer vesicle. Scale bar = 10 μm

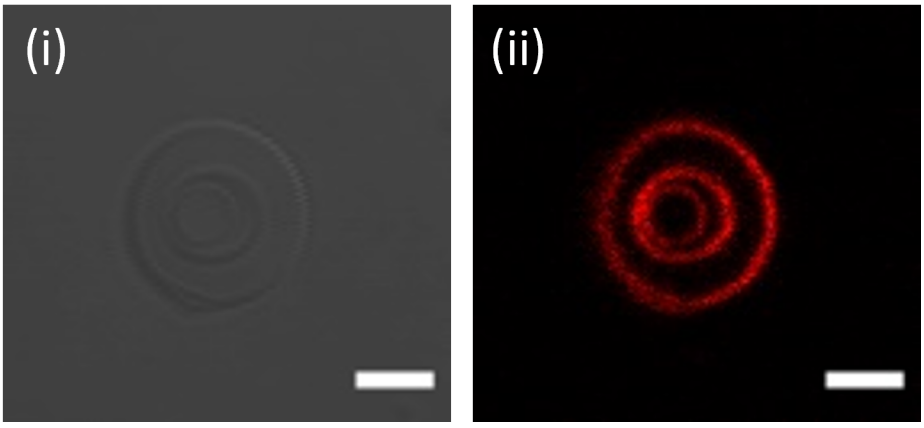

Figure S20: A few rare instances show a concentric triple vesicle morphology (vesicle-in-vesicle-in-vesicle) when the osmotic shock is given to a sGUV. Scale bar = 5 μm

REFERENCES

1. Dimova, R., N. Bezlyepkina, M. D. Jordö, R. L. Knorr, K. A. Riske, M. Staykova, P. M. Vlahovska, T. Yamamoto, P. Yang, and R. Lipowsky, 2009. Vesicles in electric fields: Some novel aspects of membrane behavior. *Soft Matter* 5:3201–3212.

2. Pan, J., T. T. Mills, S. Tristram-Nagle, and J. F. Nagle, 2008. Cholesterol perturbs lipid bilayers nonuniversally. *Physical review letters* 100:198103.

3. Henriksen, J. R., and J. H. Ipsen, 2004. Measurement of membrane elasticity by micro-pipette aspiration. *The European physical journal E* 14:149–167.

4. Meleard, P., C. Gerbeaud, T. Pott, L. Fernandez-Puente, I. Bivas, M. D. Mitov, J. Dufourcq, and P. Bothorel, 1997. Bending elasticities of model membranes: influences of temperature and sterol content. *Biophysical journal* 72:2616–2629.

5. Vlahovska, P. M., R. S. Gracia, S. Aranda-Espinoza, and R. Dimova, 2009. Electrohydrodynamic model of vesicle deformation in alternating electric fields. *Biophysical journal* 96:4789–4803.

6. Sinha, K. P., and R. M. Thaokar, 2017. Electrohydrodynamics of a compound vesicle under an ac electric field. *Journal of Physics: Condensed Matter* 29:275101.